Deliverable D 3.3
Model for the creep of refractories

Document type	**Deliverable D 3.3**
Document Version / Status	**1.3**
Primary Authors	**Alain Gasser, alain.gasser@univ-orleans.fr, UORL**
Distribution Level	**PU (Public)**
Project Acronym	**ATHOR**
Project Title	**Advanced THermomechanical multiscale mOdelling of Refractory linings**
Grant Agreement Number	**764987**
Project Website	www.etn-athor.eu
Project Coordinator	**Marc Huger, marc.huger@unilim.fr, UNILIM**
Document Contributors	**Lucas Teixeira, lucas.breder-teixeira@univ-orleans.fr, UORL** **Soheil Samadi, soheil.samadi@unileoben.ac.at, MUL**

History of Changes

Version	Date	Author (Organization)	Change	Page
1.0	30.03.2021	Lucas Teixeira (UORL), Soheil Samadi (MUL)	First draft	All
1.1	30.03.2021	Glyn Derrick (UNILIM)	English and formatting	All
1.2	31.03.2021	Alain Gasser (UORL), Lucas Teixeira (UORL), Soheil Samadi (MUL)	Scientific comments and corrections	All
1.3	21.05.2021	Lucas Teixeira (UORL), Glyn Derrick (UNILIM), Marc Huger (UNILIM)	Modification of Figure 4 and final check	All

European Commission
Horizon 2020
European Union funding
for Research & Innovation

TABLE OF CONTENTS

1 Introduction

The goal of this report is to describe the new constitutive models, developed during the project ATHOR, to simulate the creep and damage of refractories at high temperatures. In general, refractories present an asymmetric creep behaviour, i.e., different strain rate under tension and under compression, and have different failure modes depending on the stress sign.

It has been shown by [1] that, for an alumina-spinel material used in the working lining of steel ladles, it is important to consider the effects of asymmetric primary and secondary creep. This feature is not currently available in commercial finite element analysis (FEA) software such as Abaqus [2], therefore is addressed in the models proposed in this work.

2 Asymmetric creep model – Primary and secondary creep

2.1 Introduction

As it was described in detail in the deliverable 3.2 [3], the Norton-Bailey (NB) creep model is one of the most widely used models for the simulation of the creep behaviour of refractories. This is due to its simplicity and accuracy in fitting the time-strain curves observed in experiments. Equ. 1 shows the viscoplastic creep strain rate relation for the NB model:

$$\dot{\varepsilon}_{cr} = A\, \sigma_{eq}^{n}\, \varepsilon_{cr}^{m} \qquad \text{Equ. 1}$$

where ε_{cr} is the accumulated creep strain, A, n and m are temperature dependent material parameters and σ_{eq} is the von Mises equivalent stress. For the case of secondary creep, $m = 0$.

To account for the asymmetric creep of refractories under secondary creep, Blond et al. [4] extended the NB model using a split of the principal stress vectors into a positive and a negative part to propose a secondary creep model, resulting in:

$$\bar{\bar{\sigma}} = \langle \bar{\bar{\sigma}} \rangle - \langle -\bar{\bar{\sigma}} \rangle \qquad \text{Equ. 2}$$

where $\langle \bar{\bar{\sigma}} \rangle$ are the Macaulay brackets. This split results in the definition of the model in terms of independent tension and compression parameters. In this sense, the two parts of the deviatoric stress tensor are given by:

$$\bar{\bar{s}}^{\pm} = \langle \pm\bar{\bar{\sigma}} \rangle - \frac{1}{3} tr(\langle \pm\bar{\bar{\sigma}} \rangle)\, \bar{\bar{I}} \qquad \text{Equ. 3}$$

where the indexes $\pm$ indicate the positive and negative parts of the variables, respectively, and $\bar{\bar{I}}$ is the identity second order tensor. The equivalent von Mises stresses are, then:

$$\sigma_{eq}^{\pm} = \sqrt{\frac{3}{2} \bar{\bar{s}}^{\pm} : \bar{\bar{s}}^{\pm}} \qquad \text{Equ. 4}$$

European Commission | Horizon 2020 European Union funding for Research & Innovation

Resulting in a viscoplastic strain rate of the form:

$$\dot{\bar{\bar{\varepsilon}}}_{cr} = \frac{3}{2}\frac{\bar{\bar{s}}^{+}}{\sigma_{eq}^{+}}A^{+}\langle\sigma_{eq}^{+} - \sigma_{y}^{+}\rangle^{n^{+}} - \frac{3}{2}\frac{\bar{\bar{s}}^{-}}{\sigma_{eq}^{-}}A^{-}\langle\sigma_{eq}^{-} - \sigma_{y}^{-}\rangle^{n^{-}} \qquad \text{Equ. 5}$$

where $A^{\pm}$ and $n^{\pm}$ are material constants and $\sigma_y^{\pm}$ is the yield stress in tension $(+)$ and compression $(-)$.

2.2 Model description

To represent the asymmetric behaviour of refractories, Equ. 1 was adapted following the same principle of splitting the stress tensor in a positive and a negative part, as used by Blond et al. [4], while also considering the primary creep stage.

The proposed model also differentiates from Blond's model in the way the different contributions of the compression and tensile characteristics of the material are considered. After the decomposition of the stress tensor, the deviatoric and equivalent stresses are calculated for each part (positive and negative) using Equ. 3 and Equ. 4, respectively. Nevertheless, instead of using $\bar{\bar{s}}^{\pm}$ and $\sigma_{eq}^{\pm}$ to calculate directly the positive and negative viscoplastic strain rates, these values are used to calculate relative weights that each part of the stress tensor have on the total equivalent stress, using the following relationship:

$$w^{\pm} = \frac{\sigma_{eq}^{\pm}}{\sigma_{eq}^{+} + \sigma_{eq}^{-}} \qquad \text{Equ. 6}$$

Each portion of the viscoplastic strain rate is calculated as a function of the total deviatoric and equivalent stresses (using the full stress tensor, before the decomposition into positive and negative parts) and the respective material properties:

$$\dot{\bar{\bar{\varepsilon}}}_{cr}^{\pm} = f(\bar{\bar{s}}, \sigma_{eq}, A^{\pm}, n^{\pm}, m^{\pm}) \qquad \text{Equ. 7}$$

After this, each part of the viscoplastic strain rate is weighted by the values calculated using Equ. 6. Therefore, the viscoplastic strain rate of the proposed asymmetric creep model is given by:

$$\dot{\bar{\bar{\varepsilon}}}_{cr} = w^{+}\frac{3}{2}\frac{\bar{\bar{s}}}{\sigma_{eq}}A^{+}\langle\sigma_{eq} - \sigma_{y}^{+}\rangle^{n^{+}}\varepsilon_{cr}^{m^{+}} - w^{-}\frac{3}{2}\frac{\bar{\bar{s}}}{\sigma_{eq}}A^{-}\langle\sigma_{eq} - \sigma_{y}^{-}\rangle^{n^{-}}\varepsilon_{cr}^{m^{-}} \qquad \text{Equ. 8}$$

This model was implemented in an Abaqus UMAT subroutine, and an implicit integration scheme was used according to Pan et al. [7].

2.3 Model testing – Numerical simulations

To evaluate the capabilities of the asymmetric model proposed in Section 2, a set of numerical simulations is presented in the next section, in increasing order of complexity. The goal of these simulations is to verify if the model presents the expected behaviour when subjected to complex load cases. In the simulations, isotropic primary creep in compression and secondary creep in tension were considered. The material parameters used to perform these tests, related to Equ. 8, are shown in Table 1. These material parameters correspond to an approximation of the ones observed for the alumina-spinel brick at 1300 °C.

Table 1: Material parameters used in the numerical simulations.

Parameter	Compression (Primary creep)	Tension (Secondary creep)
E [MPa]	30000	30000
υ	0.2	0.2
$log_{10}A\ [MPa^{-n}s^{-1}]$	-14.16	-5.4
n	3.96	1.5
m	-2.74	$-$

In the reported simulations within this document, from the material parameters presented in Table 1, four types of model were considered:

- Abaqus symmetric creep model using the compression properties of the material. This configuration is commonly seen in publications related to the creep of refractories.
- Abaqus symmetric creep model using the tension properties of the material, used as a reference to compare with the asymmetric model.
- UMAT asymmetric creep model, using the compression properties of the material for compression and tension, to verify if the asymmetric model tends to a symmetric one when necessary.
- UMAT asymmetric creep model, using the corresponding properties for tension and compression.

2.3.1 Normal loads with stress reversal in two dimensions

The first model corresponds to a simple two-dimensional element (Figure 1-a) subjected to stresses in directions 1 and 2, according to Figure 1-b. The maximum tensile stress is $\sigma = 0.2$ MPa, and the minimum compression stress is $\sigma = -2.0$ MPa. Figure 1-c and Figure 1-d show the time periods for which the stresses are kept in the sample.

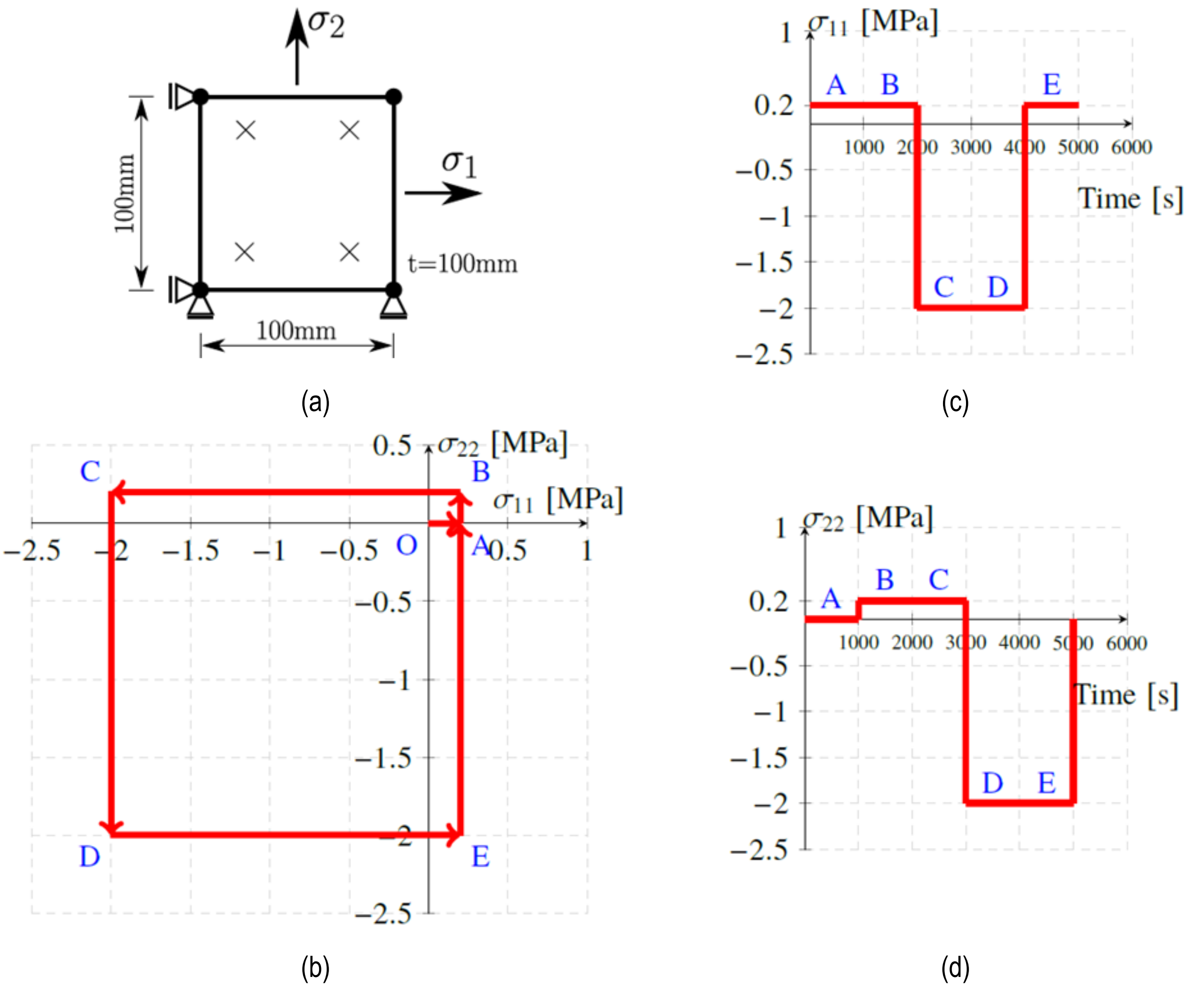

Figure 1: Stress distribution – Normal loads. (a) Simulation model. (b) Stress path. (c) σ_{11} x Time. (d) σ_{22} x Time.

Although this is a simple model, it represents a situation where, during the loading cycle, there are moments where both principal stresses are positive (Point B), both are negative (Point D), and when there is a composition of positive and negative stresses at the same integration point (Points C and E). Therefore, the model is useful to show the difference between a symmetric and an asymmetric model, as well as the effect of the loading history. For this model, an extra curve using the tension material parameters for both tension and compression material laws is also presented.

Figure 2 shows the accumulated viscoplastic strains computed in each of the situations previously described. It is possible to observe that, when the same properties are used for tension and compression, the UMAT provides the same results as a symmetric model. More importantly, the asymmetric model presents an intermediate response between the tension and the compression symmetric models, as expected.

In Figure 2, it is clear that, until approximately 30 min (represented by the subfigure placed inside Figure 2), when only tension stresses are present in the element (Points A and B in Figure 1), the symmetric and asymmetric models give the same result. From that point further, when an asymmetry is included in the loading (Point C in Figure 1), the model response changes, becoming an interpolation between the tension and compression behaviours.

European Commission
Horizon 2020
European Union funding
for Research & Innovation

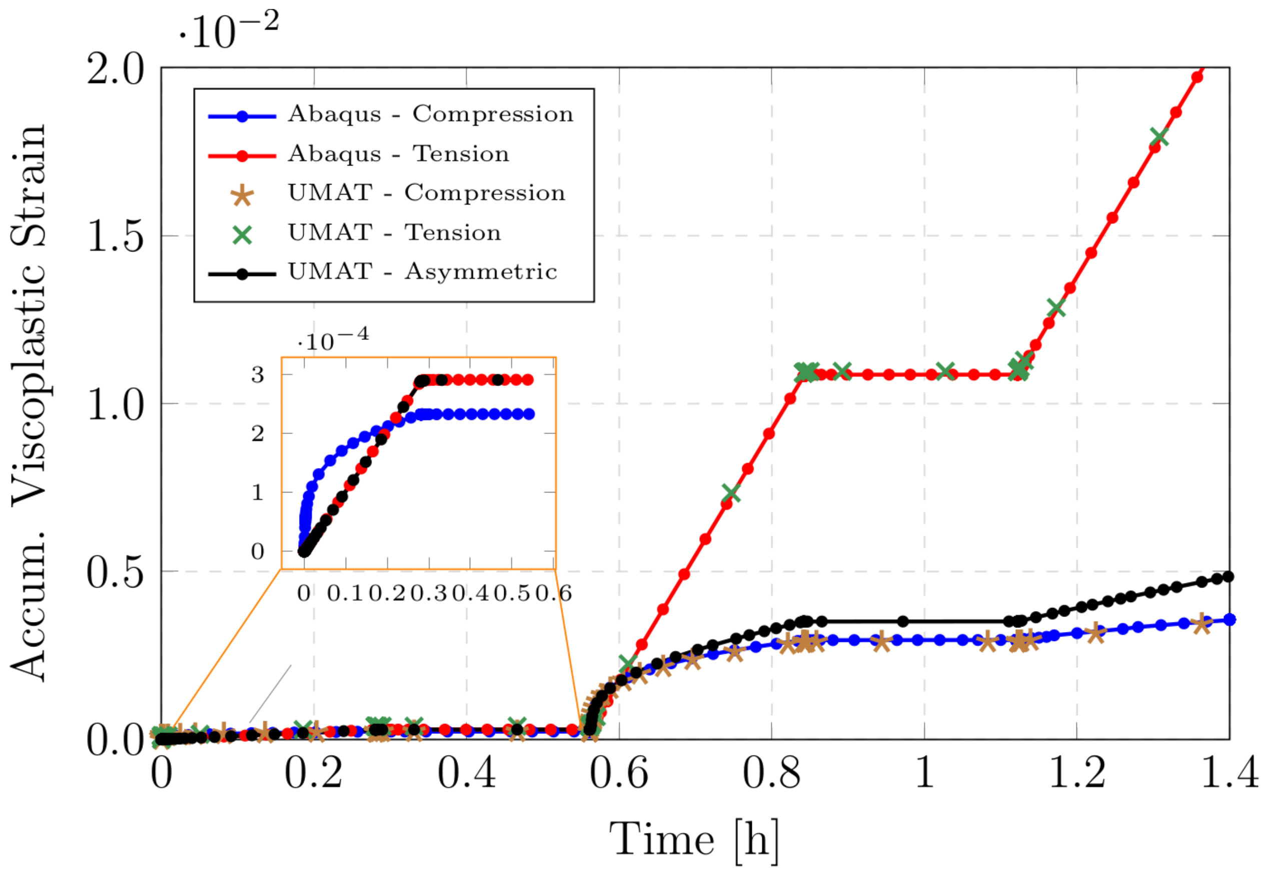

Figure 2: Accumulated viscoplastic strain - Normal loads.

2.3.2 Brazilian test

Figure 3 shows the geometry, mesh and boundary conditions used to compare the symmetric and asymmetric models for a Brazilian test. The sample was discretized using linear square elements with full integration, except for a transition zone between the refined mesh in the contact region and the rest of the geometry, where linear triangular elements with full integration were used.

The sample was considered to have a diameter of 50 mm and a thickness of 40 mm. An analytic rigid surface is used to distribute the load more evenly on the sample and to avoid excessive stress concentrations. The same strategy is used at the bottom part of the model to restrict the vertical displacement of the sample. Due to the symmetry of the geometry and of the loading, only half of the sample was modelled.

A force of -400 N was applied on the model following a 30 s linear ramp and kept for two hours, resulting in a total of -800 N for the complete geometry.

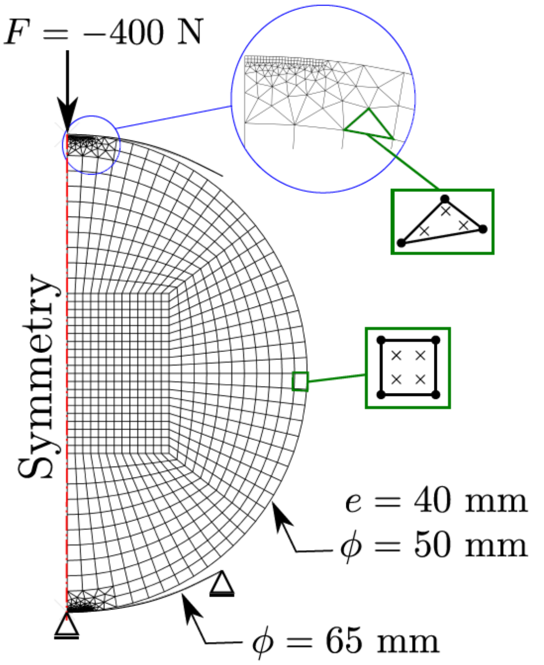

Figure 3: Brazilian test - Geometry, mesh and boundary conditions.

Figure 4 shows a comparison between vertical (*Figure 4*-a) and horizontal (*Figure 4*-b) displacements taken at different points of the sample for the four types of model.. It should be noted that vertical displacement has been taken at the centre of the sample (Point A) and that the horizontal displacement (zero in the centre) has been taken at Point B. It is possible to observe that, when compression curves are used in the asymmetric model, the result is in good agreement with the symmetric model available on the software Abaqus, and an interpolation between the tension and compression behaviours is obtained with the proposed model.

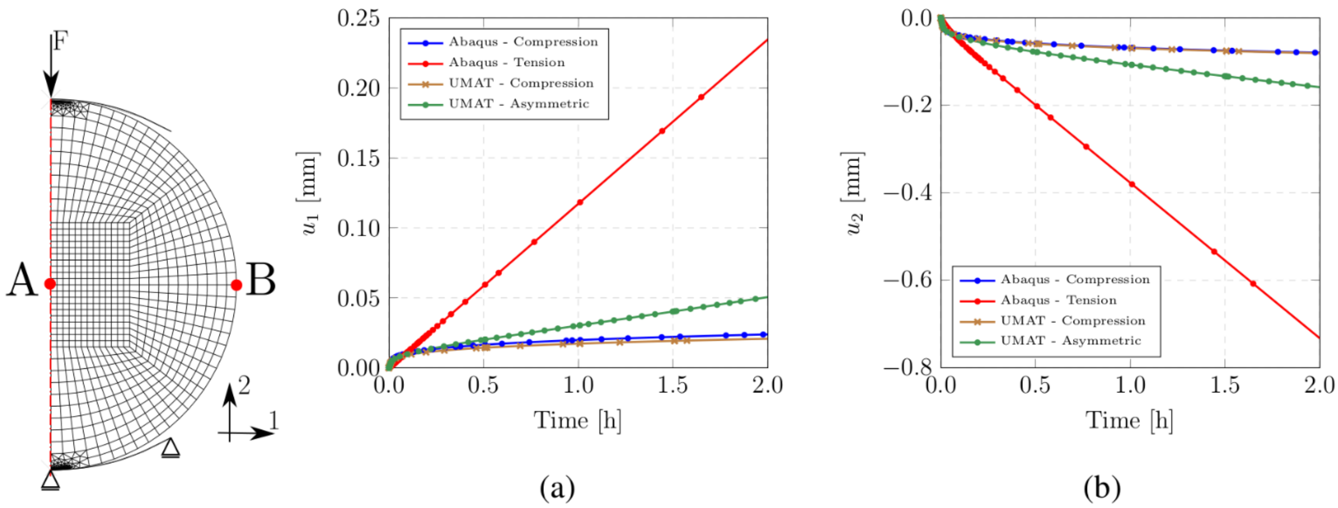

Figure 4: (a) Vertical and (b) horizontal displacements in the Brazilian test sample.

Figure 5 shows the effect of the asymmetry in the accumulated viscoplastic strain on a Brazilian test, where Figure 5-a corresponds to the case where only compression creep parameters were used, Figure 5-b corresponds to the use of tension properties and Figure 5-c corresponds to the asymmetric properties. Once again, the proposed asymmetric model shows an intermediary behaviour between the symmetric models. This clearly demonstrates the importance of considering the different material properties, in tension and in compression, since the strain plots differ considerably from the symmetric cases. In this figure, the load application regions were removed from the plots, since they correspond to stress concentration areas and tend to make the visualization more difficult.

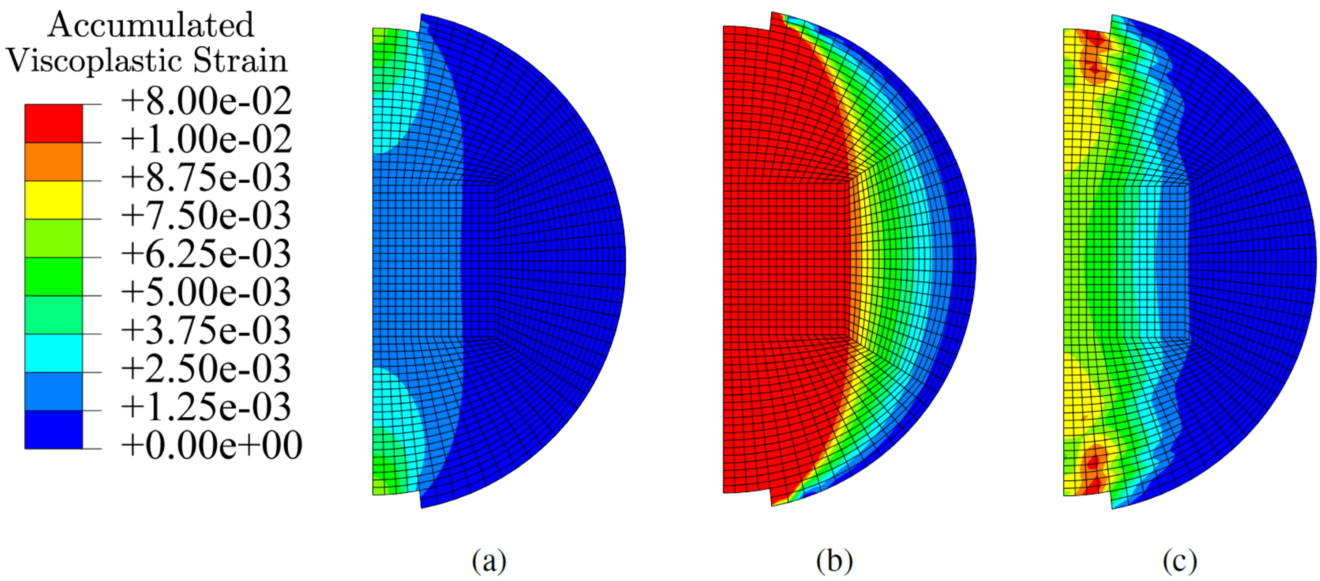

Figure 5: Accumulated viscoplastic strain distribution on a Brazilian test sample. (a) compression (b) tension and (c) asymmetric material properties.

2.3.3 Four-point bending test

The four points bending test is an interesting example because it presents tension stresses in the direction perpendicular to the loading in the lower part of the sample, and compression stresses in the upper part of the sample. Therefore, an asymmetric model is expected to present a significantly different structural response when compared with symmetric models.

In the simulated model, the height and the thickness of the sample were considered to have 30 mm, and the length 150 mm. The upper span of the load application rolls was 40 mm, and the lower span of the supports was 120 mm. Due to the symmetry of the model, half of the geometry was modelled. To limit the effect of stress concentrations in the contact region, circular analytic surfaces were used to apply the force. The force $F = -30$ N was applied as a linear ramp over 30 s and maintained for 2 hours.

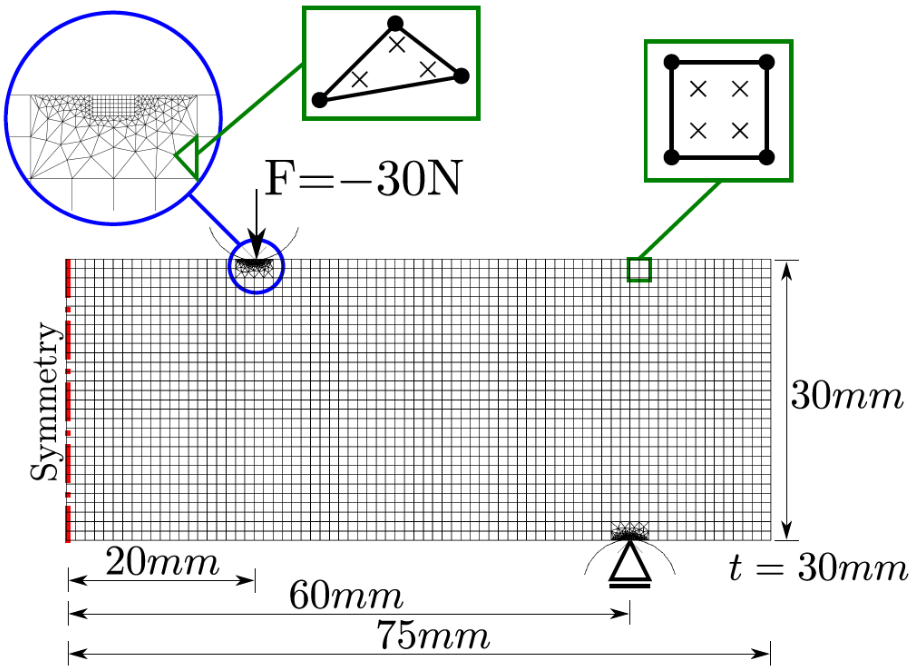

Figure 6: Four points bending test - Geometry, mesh and boundary conditions.

The mesh was composed by squared linear finite elements with full integration, except from the transition between the refined contact region to the rest of the sample, that used triangular linear elements with full integration. Although a quadratic mesh could be more suitable to simulate bending loads, a compromise needed to be made between accuracy and run time, since the asymmetric model can be time expensive. To compensate for the loss of accuracy due to the element order, a refined mesh was used, allowing for a satisfactory solution using a reasonable number of degrees of freedom.

Figure 7-a shows the difference between the symmetric and asymmetric models in the vertical displacement of the lower point over the symmetry line of the sample. It is possible to notice the similar behaviour between Abaqus and the UMAT models when symmetric compression properties are used. As expected, the asymmetric model presents a response in between the tension and compression ones.

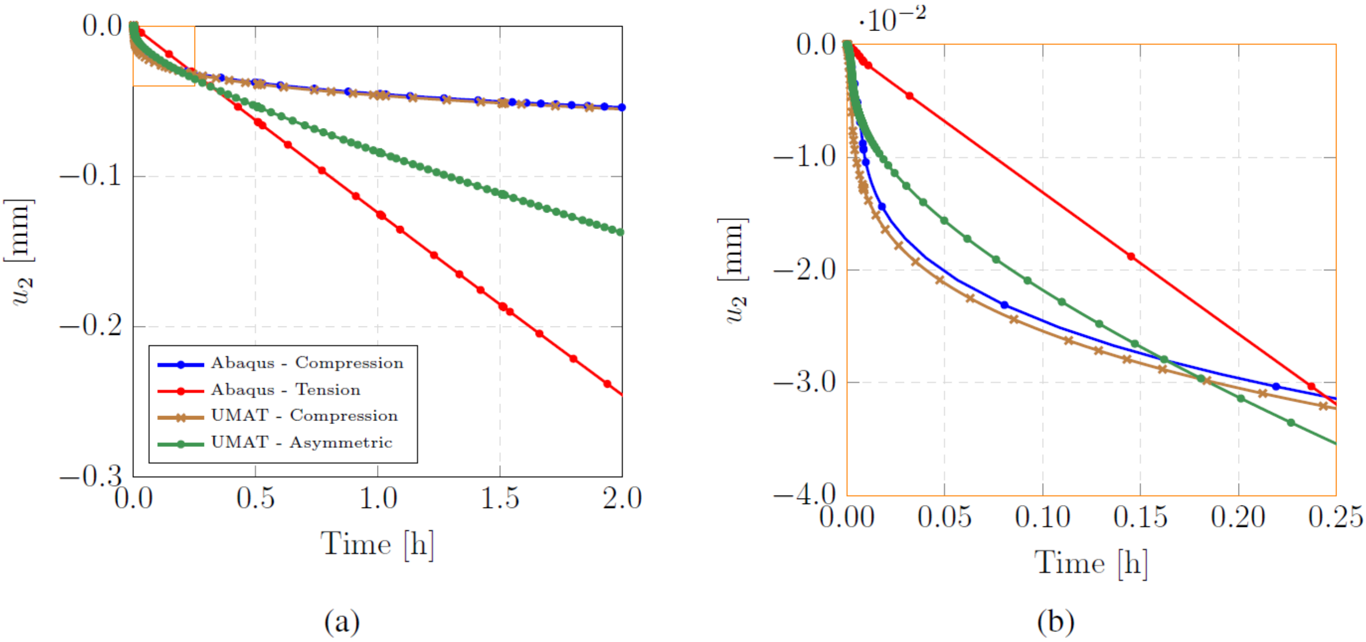

Figure 7: (a) Vertical displacement on the lower centre point of the four points bending sample. (b) Detail of the first 15 min.

Figure 7-b corresponds to a detail of the first 15 min of the simulation, showing that, at the beginning of loading, the displacement calculated using compression properties is higher than the one using tension properties, although in the overall case after 1 hour of loading this is not the situation. This comes from the fact that, in compression, a primary creep law is used, which presents a high viscoplastic strain rate at the beginning of the creep response, but that decreases rapidly over time.

Similar to what was observed on the Brazilian tests, Figure 8 shows the influence of the asymmetric nature of refractory materials on the strains distributions when complex loading conditions are applied. It is clear that the use of compression properties (Figure 8-a) largely underestimate the strains in the model, leading to erroneous assumptions about the total life of structures composed of these materials. On the other hand, the use of tensile creep properties (Figure 8-b) overestimates the values of the accumulated viscoplastic strain and can lead to predictions that are excessively rigorous.

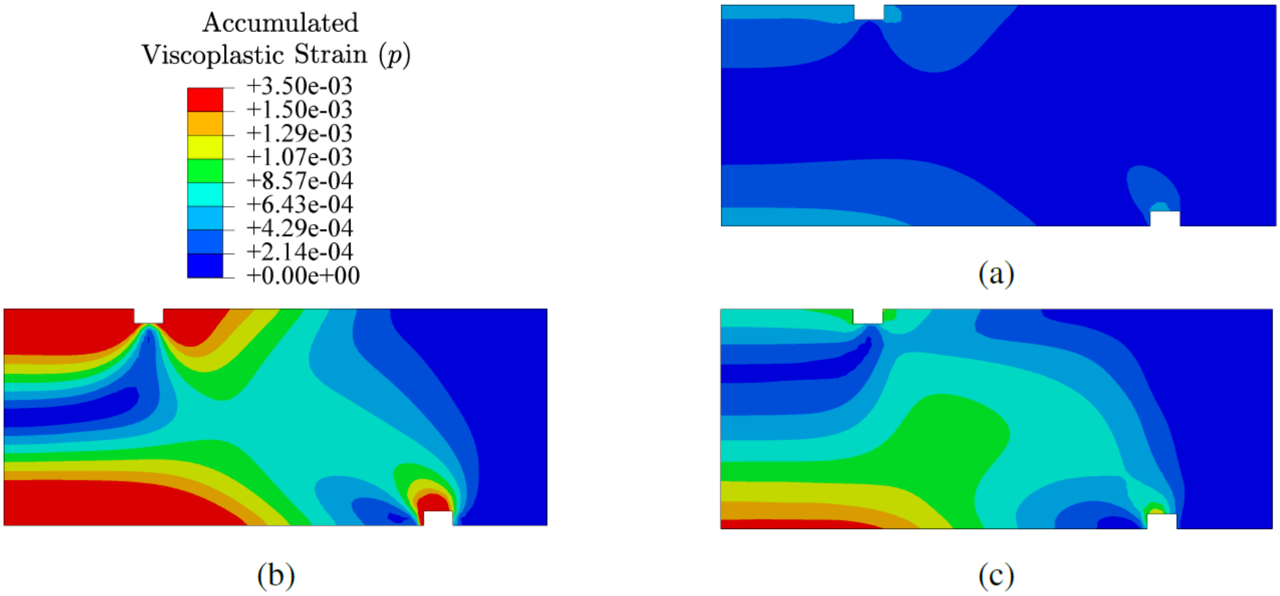

Figure 8: Distribution of accumulated viscoplastic strain on the four points bending test sample. (a) Symmetric - Compression. (b) Symmetric - Tension. (c) Asymmetric.

2.4 Identification of material parameters and model validation

In order to identify the material properties of the model presented in Section 2.2, Brazilian tests were performed at a temperature of $1300\ °C$. The open-source DIC software Ncorr [6], that implements the local subset-based reliability-guided DIC method according to Pan et al. [7], was used to calculate the full field displacements of the samples. The vertical displacement u_2 at the load application point on the sample was used as the identification target. It should be noted here that, in order to subtract the rigid body motion coming from the bottom support of the sample, this vertical displacement u_2 is corrected using the vertical displacement obtained from the contact point at the bottom of the sample.

The experimental campaign was composed of 6 tests. Nevertheless, 2 of them were considered outliers and had the results discarded, since they presented large variations in comparison with the others. The details of the experimental campaign will be discussed in further deliverables.

Even if more sophisticated identification techniques are intended to be used with the results of full field measurements, such as those based on FEMU or I-DIC [8-9], the simplified identification presented in this report is important to restrict the possible range of variation for the material parameters. When the solution space for the identification problem is complex, such as in the case of the asymmetric creep model, an unreasonably large range for the input parameters can result in excessive computational time and in convergence problems, so it is important to limit the input domain. Figure 9 shows an example of envelope for the material parameters at $1300\ °C$, obtained through a series of numerical simulations using the isotropic asymmetric creep model. During the I-DIC identifications, it can be expected that the material parameters will not highly deviate from the ones presented in the figure, even if this analysis only considers a single displacement value, and not the full field.

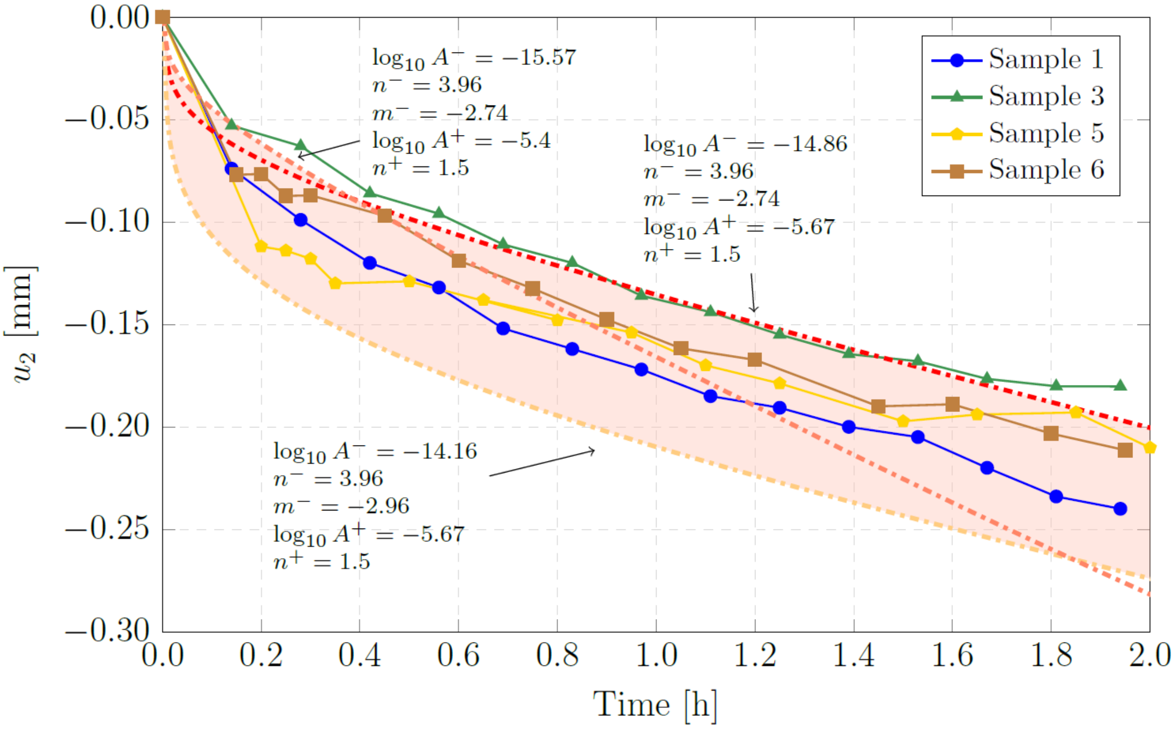

Figure 9: Vertical displacement, u_2, at loading point vs time during Brazilian tests on an Alumina Spinel sample at 1300 °C and parameters envelope.

The parameters for the alumina-spinel material were hand-fitted in order to better approximate the values of the DIC calculations, and the resulting curve is presented in Figure 10. The identified parameters were:

$$log_{10}A^- = -14.86\ MPa^{-n}s^{-1}, n^- = 3.96, m^- = -2.74, log_{10}A^+ = -5.5\ MPa^{-n}s^{-1}, n^+ = 1.5.$$

From Figure 10 it can be seen that, for the first hour of the test, the identified curve is in good agreement with the data from sample 6, while being in between samples 1 and 3. From this point, it becomes closer to sample 1, presenting a deviation of approximately 20 % in relation to samples 5 and 6 and approximately 45 % from sample 3. Sample 5 is a particular case, a higher displacement, than that of the identified curve, is present during the first half of the test, and a lower displacement in the second half.

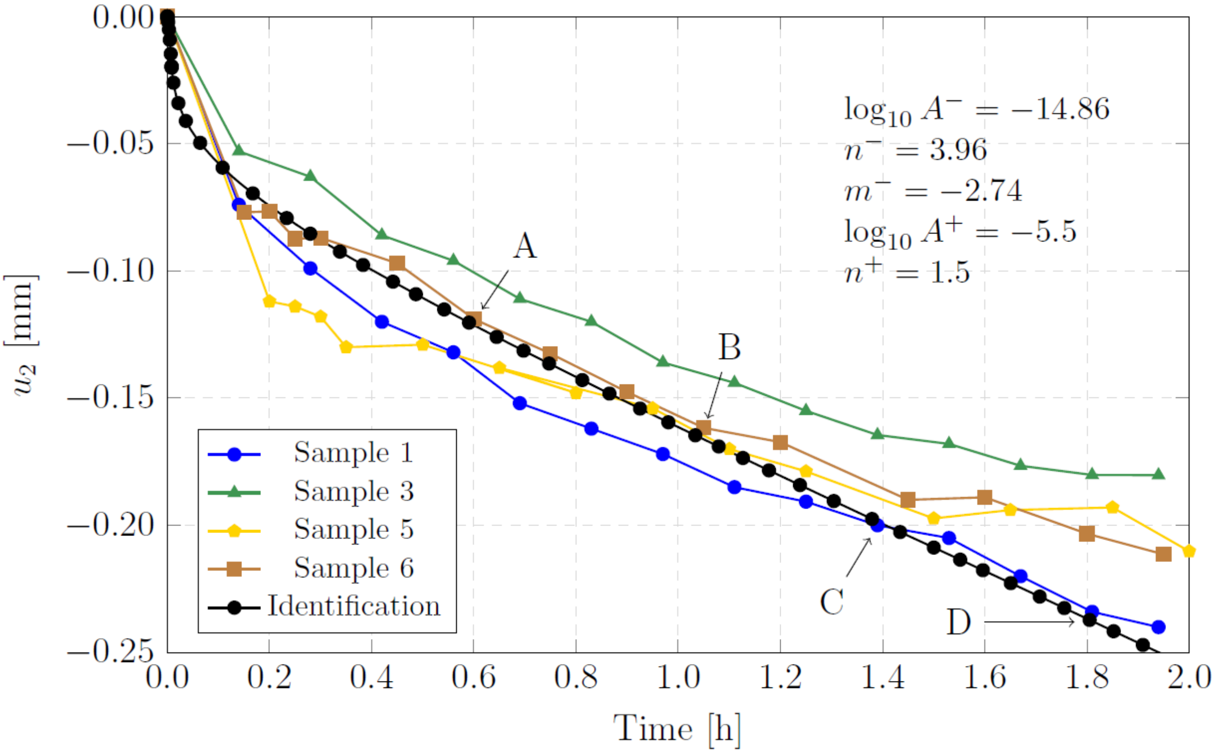

Figure 10: Inverse identification from vertical displacement, u_2, at loading point vs time during Brazilian tests on an Alumina Spinel sample at 1300 °C.

A robust way to verify the accuracy of the results obtained during the identifications is to compare the DIC displacement field with the ones resulting from the numerical simulations performed using the identified material parameters. The vertical displacements field for Points A and B on the curve represented in Figure 10, corresponding to $t = 0.6$ h and $t = 1.05$ h, respectively, are shown in Figure *11*. It is possible to see that, as has already been discussed in the literature [10], there is a rigid body rotation of the sample during the test due to imperfections in the boundary conditions, since the displacements map does not correspond to the traditional displacements field observed for Brazilian tests. To consider this effect, an extra identification calculation was made to determine the magnitude of the horizontal load in the plane of the sample that caused this deviation. A load of -7 N was identified and applied to the upper jaws during the simulation. This load corresponds to an error of $0.5°$ in the application of the load, what shows that the experimental procedure is sensitive to small deviations from the ideal boundary conditions. In this case, since the loads are not symmetric around the y axis anymore, a full geometric representation of the sample's surface was used.

Figure *12* shows the results of the numerical simulations using the previously identified material parameters and the horizontal load. It is possible to observe that the displacement maps of Figure *11* and Figure *12* have a good equivalence, despite the experimental errors and the simplicity of the identification procedure used.

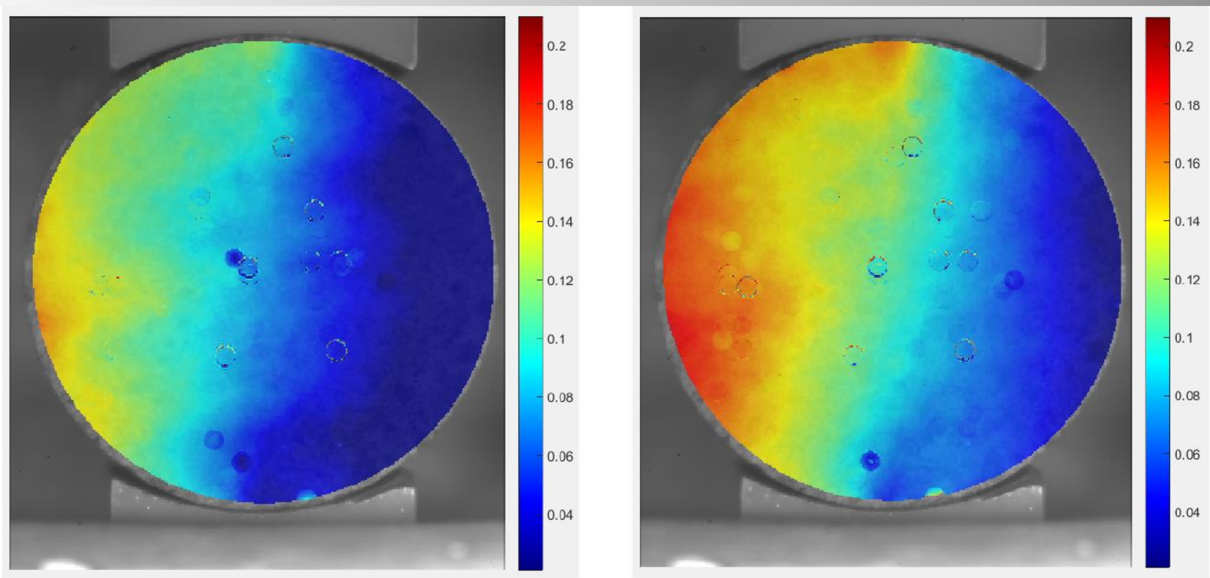

(a) (b)

Figure 11: Brazilian tests: Vertical displacement, u_2, in mm at 1300 °C - DIC sample 6. (a) Point A. (b) Point B.

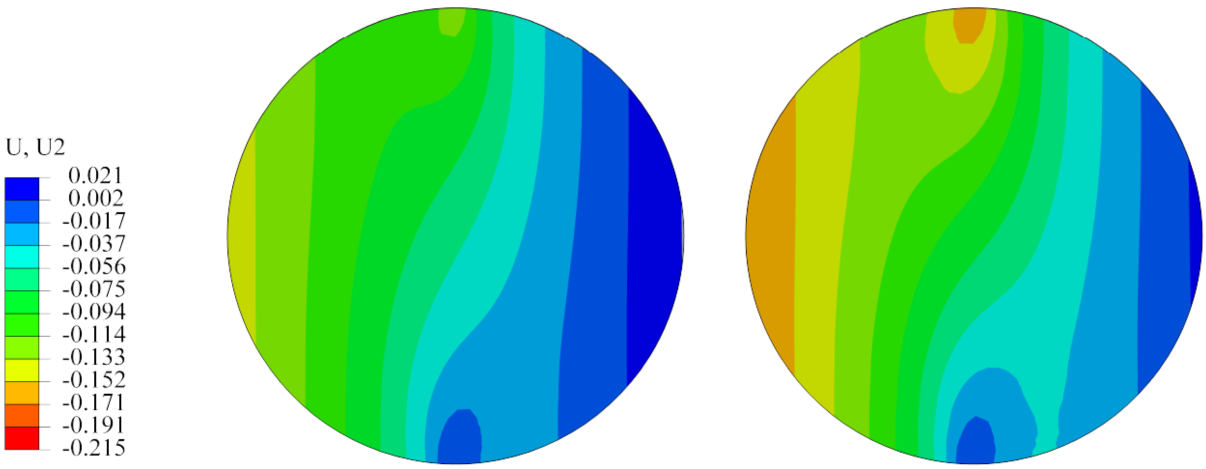

(a) (b)

Figure 12: Brazilian tests: Vertical displacement at 1300 °C - Simulation. (a) Point A. (b) Point B.

3 Combined tensile failure with creep modelling

3.1 Introduction

The Concrete Damaged Plasticity (CDP) model in Abaqus [2] has been widely applied for simulation of tensile and compressive failure phenomena in concrete and refractory fields. This model was explained thoroughly in Deliverable 3.2 [3], where two drawbacks of this material model were also mentioned. Firstly, there is a lower limit for the post-failure stress (1 % of the tensile strength) and it cannot be decreased to zero. This was shown to be a drawback in case of materials with high brittleness numbers [11]. Due the contribution of this lower limit to the energy consumption of the model, it might lead to errors in inverse evaluation of fracture parameters [11]. Secondly, creep cannot be modelled simultaneously with tensile failure in the CDP model. Since both creep and tensile failure are important causes of irreversible behaviour in refractory linings, the following constitutive material model was developed to combine their mutual influence in one model. This model, termed DECR, combines an isotropic damaged elasticity model [11] with an asymmetric Norton-Bailey type creep model.

In order to evaluate the DECR model, it was used for the simulation of wedge splitting test (WST) and inverse evaluation of fracture parameters at high temperature. The material selected for testing was shaped alumina spinel refractory. The WST is an appropriate means to study the fracture behaviour of refractories since it enables stable crack propagation on relatively large specimens [12-13]. Recently, Stückelweiger, et. al. developed an apparatus to perform WST at high temperature, which provides the opportunity to study the fracture behaviour at high temperatures [14]. In that study, a modelling approach is proposed to simulate WST at high temperatures in which fictitious crack model is considered only on the surface of the ligament and a Norton-Bailey type creep law in the bulk. It was shown that considering creep in the WST model has an influence on inverse evaluated fracture parameters [14].

3.2 Model description

In DECR, damaged elasticity and creep are coupled based on strain splitting assumption, i.e. the strain is divided between creep and damaged elasticity using the same stress. The 2nd order total strain tensor ($\bar{\bar{\varepsilon}}_{tot}$) is decomposed into two parts (Equ. 9), reversible ($\bar{\bar{\varepsilon}}_{r}$) and irreversible ($\bar{\bar{\varepsilon}}_{ir}$) strain tensors. The reversible strain tensor includes both elastic ($\bar{\bar{\varepsilon}}_{el}$) and damage ($\bar{\bar{\varepsilon}}_{d}$) strain tensors, and the irreversible strain tensor refers to the creep strain. The model has been modified such that the damage strain is used in the definition of softening curve and the calculation of damaged stiffness of the material. Also, as both elastic and damage strains are reversible, a different physical outcome is not observed.

$$\bar{\bar{\varepsilon}}_{tot} = \bar{\bar{\varepsilon}}_{r} + \bar{\bar{\varepsilon}}_{ir} = (\bar{\bar{\varepsilon}}_{el} + \bar{\bar{\varepsilon}}_{d}) + \bar{\bar{\varepsilon}}_{cr} \qquad \text{Equ. 9}$$

The creep model is a Norton-Bailey type creep model developed based on the existing model in Abaqus software [2] in which the creep strain rate ($\dot{\varepsilon}_{cr}$) is a function of the equivalent von Mises stress (σ_{eq}) and the accumulated creep strain (ε_{cr}) as Equ. 10.

$$\dot{\varepsilon}_{cr} = (\mathrm{a}\,{\sigma_{eq}}^{b}[(c+1)\,\varepsilon_{cr}]^{c})^{\frac{1}{c+1}} \qquad \text{Equ. 10}$$

where a, b, and c are the creep parameters, obtained using an inverse evaluation algorithm and creep experiments, as explained in Ref. [15]. It should be noted that Equ. 10 is equivalent to Equ. 1, but Abaqus uses a different representation of the Norton-Bailey law, which was also used in the development of the DECR model. The equivalent von Mises stress is calculated as follows:

$$\sigma_{eq} = \sqrt{\frac{3}{2}\bar{\bar{\sigma}}:\bar{\bar{\sigma}}} \qquad \text{Equ. 11}$$

In the current model, only the primary creep stage is considered for the creep behaviour of the refractory. This assumption is plausible due to the comparably short duration of WST, but it needs to be changed for applications in lining simulation. Furthermore, a simple assumption is considered for asymmetric creep behaviour definition, which is based on the principal stresses (σ_P) according to Equ. 12.

$$\sigma_{\max P} \geq \sigma_{mid\,P} \geq \sigma_{\min P} \rightarrow \begin{cases} \dot{\varepsilon}_{cr} = (a^{-}{\sigma_{eq}}^{b^{-}}[(c^{-}+1)\varepsilon_{cr}]^{c^{-}})^{\frac{1}{c^{-}+1}} & if\ |\sigma_{\max P}| < |\sigma_{\min P}| \\ \dot{\varepsilon}_{cr} = \left(a^{+}{\sigma_{eq}}^{b^{+}}[(c^{+}+1)\varepsilon_{cr}]^{c^{+}}\right)^{\frac{1}{c^{+}+1}} & if\ |\sigma_{\max P}| \geq |\sigma_{\min P}| \end{cases} \qquad \text{Equ. 12}$$

Where subscripts $-$ and $+$ are for compressive and tensile creep parameters, respectively. In the case that $\sigma_{\max P} = \sigma_{mid\,P} = \sigma_{\min P}$, the sign of the principal stresses defines the compressive or tensile case. This criterion is defined specifically for the simulation of the wedge splitting test, since it is easy to implement in the model. However, refractory materials present more complicated creep behaviour in application under multiaxial stress states, which require further investigations.

A forward explicit method is employed for calculation of the equivalent creep strain increment ($\Delta\varepsilon_{cr,t}$) after integration of Eq. 10, giving Eq. 13.

$$\Delta\varepsilon_{cr,t+\Delta t} = [\left(\frac{a\sigma_{eq,t}^{b}}{c+1}\right)^{\frac{1}{c+1}} \Delta t + \varepsilon_{cr,t}{}^{\frac{1}{c+1}}]^{c+1} - \varepsilon_{cr,t} \qquad \text{Equ. 13}$$

where $\sigma_{eq,t}$ denotes the stress from the last increment. Subsequently, using a flow rule, the creep strain tensor is calculated as follows:

$$\bar{\bar{\varepsilon}}_{cr,t+\Delta t} = \bar{\bar{\varepsilon}}_{cr,t} + \Delta\varepsilon_{cr,t+\Delta t}\frac{\bar{\bar{s}}_{t}}{q_{t}} \qquad \text{Equ. 14}$$

where $\bar{\bar{s}}_{t}$ refers to the 2nd order deviatoric stress tensor at the beginning of the increment. In the next step, according to Equ. 9, the rest of the strain increment tensor is allocated to the reversible strain tensor, which is used to check whether the tensile failure occurs or not as explained in the following.

At first, a schematic of the damaged elasticity model with bilinear softening law is shown in Figure 13 [11]. In this figure the model parameters are the initial Young's modulus (E_0), tensile strength (f_t), fracture energy (G_f), and ratio constants R_1 and R_2.

Furthermore, E_{d} denotes the damaged Young's modulus, $\varepsilon_{d,ult}$ is the ultimate equivalent damage strain, and σ_{ult} is the lower post-failure stress limit, set to 0.0001% of the tensile strength.

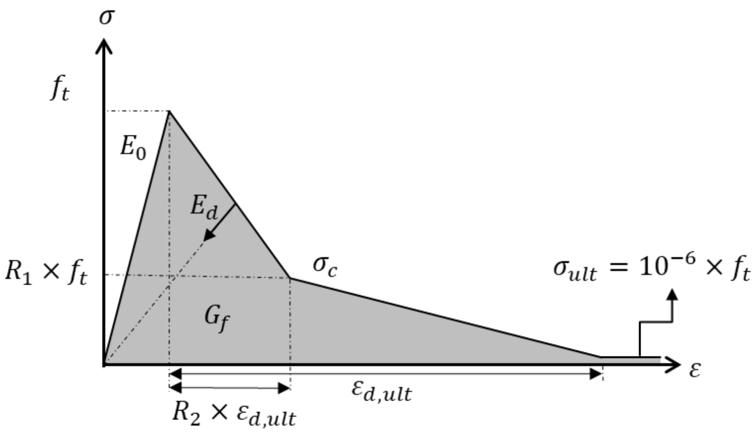

Figure 13: DE model with bilinear softening law [11]

In this model, the tensile failure starts to occur when the maximum principal stress reaches the tensile strength. Before that, the material behaves elastically. After tensile failure, with increasing of strain, maximum principal stress follows a softening curve (σ_c), which is a function of damage strain ε_d (Equ. 15). Here, the softening curve is chosen to be in bilinear form since it showed better fittings to experimental results in previous studies [11-12].

$$\sigma_{\max P} \leq \sigma_c(\varepsilon_d) \qquad \text{Equ. 15}$$

Another important underlying assumption is that the damage strain is reversible. Finally, the damage is considered isotropic, i.e. the same stiffness is assumed for all directions according to Equ. 16.

$$E_d = E_0(1 - D) \qquad \text{Equ. 16}$$

where D is the damage variable. Finally, the Yield surface of the model in two-dimensional principal stress space is shown in Figure 14. In this figure, the patterned region is the feasible region for the stress state and the two different patterns show the asymmetric creep assumption stated in Equ. 12. If the $\sigma_{\max P}$ reaches the material tensile strength, yielding occurs. The DECR model was developed as a UMAT subroutine to be used as a supplementary material for simulation in Abaqus software [2].

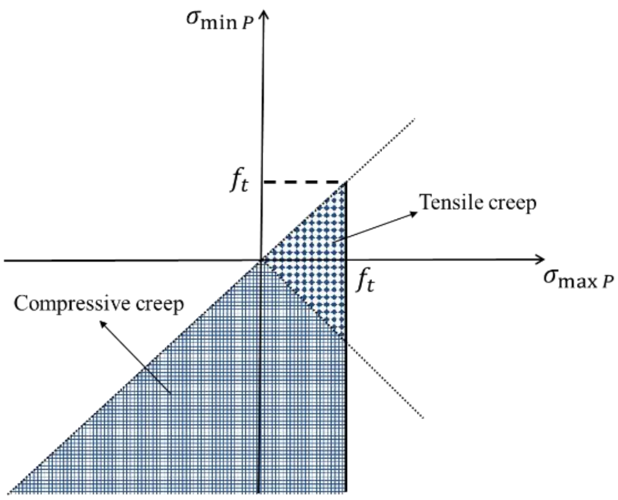

Figure 14: Yield surface in the two-dimensional principal stress space.

3.3 Damaged Elasticity and Creep model testing

A 3D single unit element was used to test the Damaged Elasticity and CReep (DECR) model. The loading steps (each with 100 s duration) were defined as follows:

1. Tensile stress loading (50 MPa)
2. No load
3. Linear increase of tensile strain to 0.003
4. Keeping the tensile strain constant at 0.003.

The assumed material parameters were: $E = 100\ GPa$, $G_f = 2e^5 N/m$, $f_t = 100\ MPa$, $R_1 = R_2 = 0.5$, $a^- = a^+ = 1e^{-16}$, $b^- = b^+ = 1.5$, and $c^- = c^+ = -0.8$.

In Figure 15, the stress and strain results of the three models (DECR, CDP and the Norton-Bailey creep model) are compared. Due to the loading definitions, the stress responses for steps 1 and 2, and total strain responses for steps 3 and 4 were the same for all models. The irreversible strain in case of DECR and Norton-Bailey creep is the strain due to creep but in the case of the CDP model, it is the strain due to damage. It was shown that the DECR subroutine and the Norton-Bailey creep model produce equal results before tensile failure, as intended. Furthermore, in the third step, after the tensile failure, in the model with the DECR subroutine, stress decreases according to the softening law; therefore, the irreversible strain (creep strain) does not increase as much as it does in the Norton-Bailey creep model, since the creep strain has a direct correlation to the stress magnitude. During the last step, higher relaxation was received in the case of Norton-Bailey creep model. In CDP model, fracture begins earlier in the third step because there is no creep influence, and the stress drops to a lower value than in DECR. The damage strain is irreversible, and no relaxation occurs in CDP.

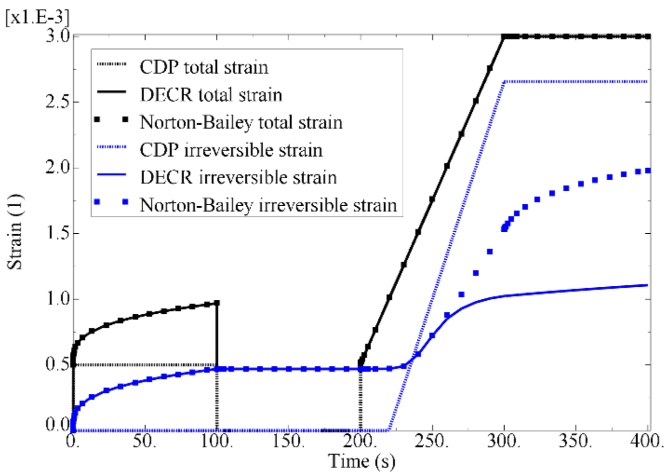

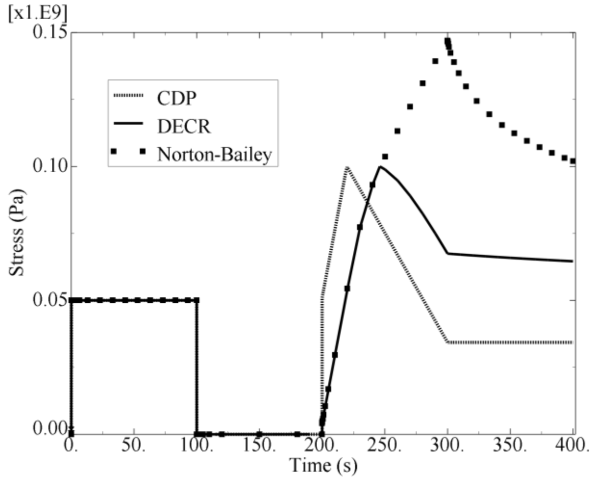

Figure 15: Material model testing and comparison using a single element model (DECR subroutine, CDP and Norton-Bailey creep models)

3.4 Wedge Splitting test simulation using the Damaged Elasticity and Creep model

According to the actual experiment design, which has been described in Deliverable 1.4 [16], a two-dimensional model of the WST specimen was built using plane strain elements [11]. The thickness of the specimen is 75 mm. Due to symmetry of the specimen and loading conditions, half of the specimen is modelled (Figure 16). A trapezoid was used to represent the transmission part made of corundum with 300 GPa Young's modulus. The wedge was modelled using an analytical rigid part. The 2D dimension of the half WST specimen is 100×50 mm² with a ligament of 1.5×66 mm². The wedge moved downwards with a constant speed of 0.5 mm/min according to the experiment. Frictionless contacts were applied between the wedge and the transmission part, as well as between the transmission part and the specimen.

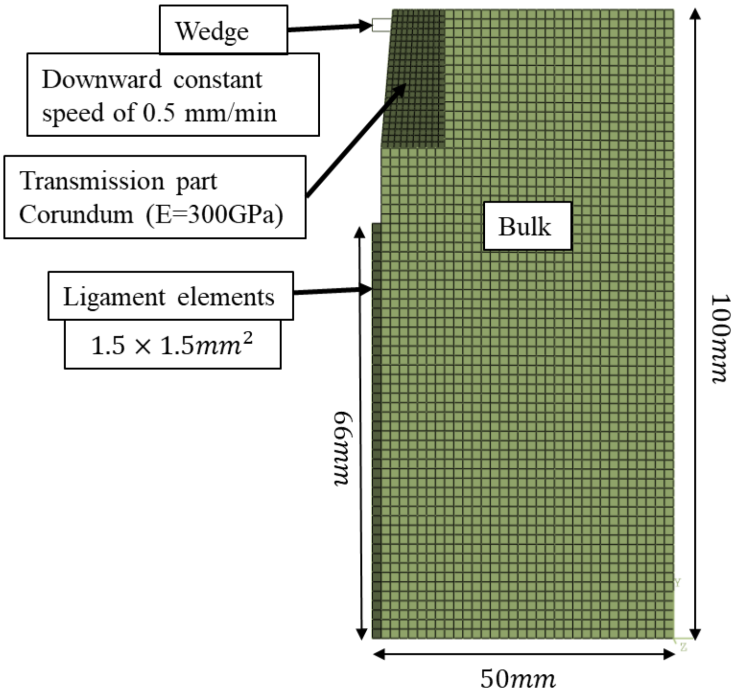

Figure 16: WST specimen 2D symmetrical model [11].

In the next step, the test results were used together with the model of WST to inverse evaluate the fracture parameters of the shaped alumina spinel refractory. The material constitutive models used for the bulk and ligament are shown in Table 2, Case 1 with the DECR model in the ligament and Case 2 with the CDP model in the ligament. The tensile failure was only considered for the ligament and not in the bulk, in order to guide the macroscopic crack to propagate in the ligament similar to the experiment where it is guaranteed by applying pre-cut lateral notches on the specimen.

Table 2: Type of model assigned to the two different parts of the WST model

	Case 1	Case 2
Ligament	DECR subroutine	CDP model
Bulk	Asymmetric creep subroutine	Asymmetric creep subroutine

In Table 3 the primary creep stage parameters obtained from previous studies for the shaped alumina spinel refractory at 1200 °C are reported [15, 17]. Compressive creep parameters were linearly extrapolated from parameters of other higher temperatures. An adaptive nonlinear least-square minimization algorithm, termed NL2SOL, implemented in the open source code DAKOTA [18], was used for inverse evaluation of fracture parameters.

Table 3: Creep model parameters used in the bulk part of the sample for WST simulation and inverse evaluation

	b	c	$a[Pa^{-n}s^{-1}]$
Compressive creep	1.60	-0.78	5.07e^{-15}
Tensile creep	1.44	-0.47	8.82e^{-14}

A comparison of models in fitting the WST results is shown in Figure 17. It was observed that Case 1 with the DECR model generated a better fit to the experimental curve compared to the Case 2 with CDP model, especially to the tail of the curve. This was also observed in two further experiments. The R-squared (R^2) average value (average of three experimental curves) was 0.993 for case 1 and 0.989 for case 2. The average of the inverse evaluated parameters are listed in Table 4. It was observed that with DECR, the fracture energy was evaluated 17 % higher than with CDP. The reason is that in CDP, the post-peak failure limit does not allow the load to decrease to zero and it adds to the consumed energy.

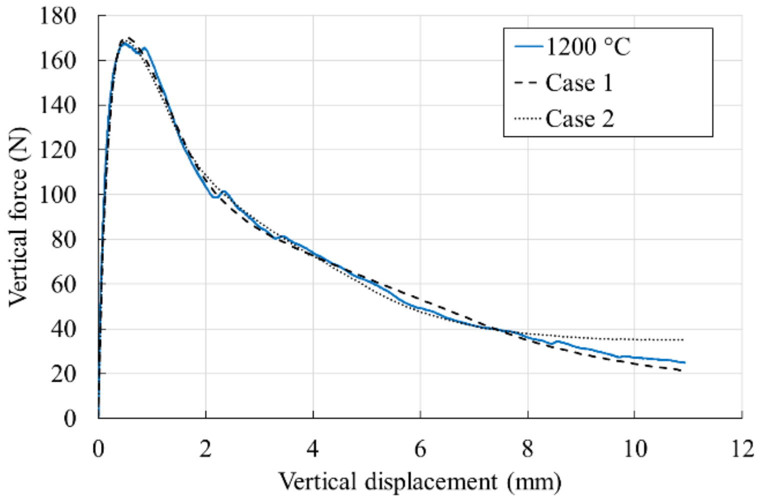

Figure 17: Inverse identified curve of the WST result using the DECR and CDP models

Table 4: Comparison of inversely evaluated fracture parameters (average of three WST results) using the DECR and CDP models

Case 1 (DECR + Creep)					Case 2 (CDP + Creep)				
G_f (N/m)	f_t (MPa)	R_1	R_2	R^2	G_f (N/m)	f_t (MPa)	R_1	R_2	R^2
296.0	1.68	0.286	0.188	0.993	253.2	1.65	0.260	0.240	0.989

In order to check the functionality of the asymmetric creep assumption, the creep state of the elements is shown in Figure 18, the colours blue and red were assigned to compressive and tensile creep states, respectively. Four different time points were selected from the test shown in Figure 17. It is shown that the area close to fracture process zone was affected by tensile creep, and it enlarged with the crack propagation. The damaged elements in the ligament were checked for these time points. At $t = 30$ s, 27% of the ligament, and at $t = 70$ s, 82% of it were damaged. At $t = 210$ s, all the ligament elements were damaged, but the traction in first element dropped to zero at t=880s, and at 23% of maximum load. It explains that the interaction between creep and fracture continues for a long time even in the first element. The curve fitting was also carried out, without considering the creep, to calculate the creep energy consumption. On average, 13% of the energy was consumed by creep at 1200 °C. Nevertheless, this ratio is only valid for the investigated material under the specific WST loading conditions.

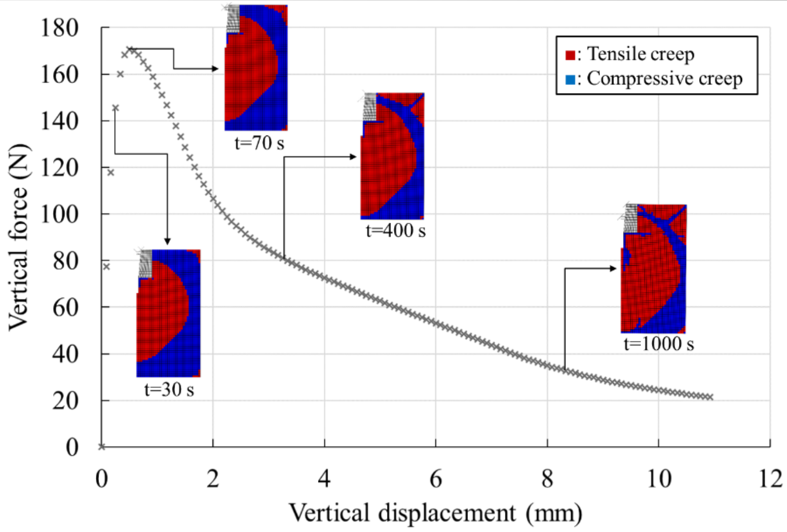

Figure 18: Compressive and tensile creep regions during WST at 1200 °C.

4 Conclusion

Two new material constitutive models were developed during the project ATHOR.

The first model uses a split of the stress tensor to calculate a weighted creep strain rate, which takes into account the primary and secondary creep behaviour of refractories. This model showed to be effective for complex load paths, being suitable for the application to real structures at high temperature. The model parameters for an alumina-spinel brick could be identified using Brazilian tests, fitting the vertical displacements of the load application point, and were validated using the full field measurement obtained using a DIC software.

The second model combines an isotropic damaged elasticity model with an asymmetric Norton-Bailey creep law. The goal of the model is to study the interaction between fracture and creep in refractory materials with the aid of the wedge splitting test. Firstly, the model subroutine was tested with single element model. It was observed that before tensile failure, the model shows the same behaviour as the Norton-Bailey creep model in Abaqus. After tensile failure, degradation of material stiffness starts and the stress decreases in presence of creep, which consumes some energy and slows down the damage rate. Nevertheless, the influence of creep on fracture depends on the loading rate. The result of a wedge splitting test performed on a shaped alumina spinel refractory at 1200 °C was chosen to test the application of the model for inverse evaluation of fracture parameters. Better fittings could be achieved using the DECR model compared to CDP model, especially to the tail of the curves due to the post-peak lower stress limit in CDP. The creep energy consumption was about 13% of the total fracture energy. Finally, it should be mentioned that further improvements are necessary for the model in order for it to be suitable for simulation of refractory linings.

5 References

[1] Teixeira, L., Samadi, S., Gillibert, J., Jin, S., Sayet, T., Gruber, D., Blond, E. Experimental Investigation of the Tension and Compression Creep Behaviour of Alumina-Spinel Refractories at High Temperatures. Ceramics, 3(3) (2020), 372 - 383. https://doi.org/10.3390/ ceramics3030033

[2] ABAQUS (2018) 'ABAQUS Documentation', Dassault systems, Providence, RI, USA.

[3] S. Samadi, L. Teixeira, G. Derrick, D. Gruber, "ATHOR Project - Deliverable D3.2: benchmark of the different thermomechanical behaviour models in commercial software applied to refractories", 2020.

[4] Blond, E., Schmitt, N., Hild, F., Blumenfeld, P., & Poirier, J. Modelling of high temperature asymmetric creep behavior of ceramics. Journal of the European Ceramic Society, 25(11) (2005), 1819 - 1827. https://doi.org/10.1016/j.jeurceramsoc.2004.06.004

[5] Benallal, A., Billardon, R., Doghri, I. An integration algorithm and the corresponding consistent tangent operator for fully coupled elastoplastic and damage equations. Communications in Applied Numerical Methods. Vol 4, Issue 6 (1988), 731-740.

[6] Blaber, J., Adair, B., Antoniou, A. Ncorr: Open-Source 2D Digital Image Correlation Matlab Software. Experimental Mechanics, 55(6) (2015), 1105-1122. https://doi.org/10.1007/s11340-015-0009-1

[7] Pan, B. Reliability-guided digital image correlation for image deformation measurement. Applied Optics, 48(8) (2009), 1535 - 1542. https://doi.org/10.1364/AO.48.001535

[8] Mathieu, F., Leclerc, H., Hild, F., Roux, S. Estimation of Elastoplastic Parameters via Weighted FEMU and Integrated-DIC. Experimental Mechanics, 55(1) (2015), 105–119. https://doi.org/10.1007/s11340-014-9888-9

[9] Hild, F., & Roux, S. Digital Image Correlation: From Displacement Measurement to Identification of Elastic Properties - a Review. Strain, 42(2) (2006), 69–80. https://doi.org/10. 1111/j.1475-1305.2006.00258.x

[10] de Melo, C. C., Furlan, M., Hild, F., Schmitt,N., Canto, R. B. Uniaxial compression test on ceramic green compact with bending consideration using digital image correlation. Powder Technology, 376 (2020), 136-148. https://doi.org/10.1016/j.powtec.2020.08.002

[11] S. Samadi, S. Jin, D. Gruber, H. Harmuth, “A comparison of two damage models for inverse identification of mode Ⅰ fracture parameters: case study of a refractory ceramic”, International Journal of Mechanical Sciences, 197 (2021), https://doi.org/10.1016/j.ijmecsci.2021.106345

[12] S. Jin, D. Gruber, and H. Harmuth, “Determination of Young’s modulus, fracture energy and tensile strength of refractories by inverse estimation of a wedge splitting procedure”, Engineering Fracture Mechanics, 116 (2014), 228–236, https://doi.org/10.1016/j.engfracmech.2013.11.010

[13] H. Harmuth, K. Rieder, M. Krobath, E. Tschegg, “Investigation of the nonlinear fracture behaviour of ordinary ceramic refractory materials”, Materials Science and Engineering: A, 214 (1996), 53–61. https://doi.org/10.1016/0921-5093(96)10221-5

[14] M. Stückelschweiger, D. Gruber, S. Jin, H. Harmuth, “Wedge-Splitting Test on Carbon-Containing Refractories at High Temperatures”, Applied Science, 9 (16) (2019) doi: 10.3390/app9163249.

[15] S. Samadi, S. Jin, D. Gruber, H. Harmuth, and S. Schachner, “Statistical study of compressive creep parameters of an alumina spinel refractory”, Ceramics International, 46 (10) (2020), 14662–14668 https://doi.org/10.1016/j.ceramint.2020.02.267

[16] H.T. Nguyen, S. Samadi, L. Teixeira, F. Asadi, R. Kaczmarek, I. Kielibla, V. Tadaion, T. Tonnesen, E. Blond, M. Huger, D. Gruber, “Deliverable D1.4: devices for mechanical characterisation at laboratory scale that are operational”, 2019.

[17] S. Samadi, L. Teixeira, S. Jin, D. Gruber, and H. Harmuth, “Creep parameter determination of a shaped alumina spinel refractory using statistical analysis”, in Proceedings of 63rd International Colloquium on Refractories, Raw Materials and Reuse, (2020), 1–5.

[18] “DAKOTA, User’s Manual.” Unlimited Release, Version 5.2, (2011).

European Commission
Horizon 2020
European Union funding
for Research & Innovation